

# Scan-matching of panoramic 2D range scans

Alexandros Filotheou, Antonis Dimitriou, Georgios Sergiadis

**Abstract**—A method for matching coplanar 2D range scans extracted from a LIDAR sensor whose field of view is  $2\pi$  is proposed. The method exploits properties of the Fourier transform that arise due to the periodicity of the range signal. Matching is performed in a correspondenceless manner. The afforded robustness and the increased accuracy compared to established scan-matching methods is exhibited through experiments. The source code is available for download.

**Index Terms**—Scan-matching, localisation, panoramic LIDAR

## I. INTRODUCTION

Contribution: invariant to large angular errors

## II. PROBLEM FORMULATION

**Problem I.** Let a mobile robot, capable of motion in the  $x$ - $y$  plane, be equipped with a coplanarly mounted range scan sensor emitting  $N_s$  rays. Let also the following be available or standing:

- The field of view of the range sensor is  $360^\circ$
- A 2D range scan  $\mathcal{S}_0$ , captured at time  $t_0$
- A 2D range scan  $\mathcal{S}_1$ , captured at  $t_1 \geq t_0$

Then the objective is estimating the 3D rigid body transformation  $T = (\Delta x, \Delta y, \Delta \theta)$  which, when applied to the endpoints of  $\mathcal{S}_1$ , aligns them to those of  $\mathcal{S}_0$  with the least error.

## III. DEFINITIONS

**Definition I.** *Definition of a range scan captured from a conventional 2D LIDAR sensor.* A conventional 2D LIDAR sensor provides a finite number of ranges, i.e. distances to objects within its range, on a horizontal cross-section of its environment, at regular angular and temporal intervals, over a defined angular range [11]. We define a range scan  $\mathcal{S}$ , consisting of  $N_s$  rays over an angular range  $\lambda$ , to be an ordered map  $\mathcal{S} : \Theta \rightarrow \mathbb{R}_{\geq 0}$ , where  $\Theta = \{\theta_n \in [-\frac{\lambda}{2}, +\frac{\lambda}{2}) : \theta_n = -\frac{\lambda}{2} + \lambda \frac{n}{N_s}, n = 0, 1, \dots, N_s-1\}$ . Angles  $\theta_n$  are expressed relative to the sensor's heading, in the sensor's frame of reference.

**Definition II.** A LIDAR sensor's angle increment  $\gamma$  is the angular distance between two consecutive rays:  $\gamma \triangleq \frac{\lambda}{N_s}$

This work was supported by the European Union and Greek National Funds through the Operational Program Competitiveness, Entrepreneurship, and Innovation, under the call Research Create Innovate under Project T2EDK-02000. Corresponding author: Alexandros Filotheou, [alefilot@auth.gr](mailto:alefilot@auth.gr). The authors are with the Department of Electrical and Computer Engineering, Aristotle University of Thessaloniki, 54124 Thessaloniki, Greece

**Definition III.** *Scan-matching (or scan-to-scan matching) using a 2D LIDAR sensor* (adapted for use in two dimensions from [4]). Let two range scans as defined by Definition I,  $\mathcal{S}_R$  and  $\mathcal{S}_V$ , be captured from a LIDAR sensor operating in the same environment at both capturing times. Let  $p_V(x_V, y_V, \theta_V)$  be the pose from which the sensor captured  $\mathcal{S}_V$ , expressed in some coordinate system (usually a past pose estimate of the sensor). The objective of scan-matching in two dimensions is to find the roto-translation  $\mathbf{q} = (\mathbf{t}, \theta)$ ,  $\mathbf{t} = (\Delta x, \Delta y)$  that minimises the distance of the endpoints of  $\mathcal{S}_V$  roto-translated by  $\mathbf{q}$  to their projection on  $\mathcal{S}_R$ . Denoting the endpoints of  $\mathcal{S}_V$  by  $\{p_V^i\}$ , in formula:

$$\min_{\mathbf{q}} \sum_i \left\| p_V^i \oplus \mathbf{q} - \prod \{\mathcal{S}_R, p_V^i \oplus \mathbf{q}\} \right\|^2 \quad (1)$$

The symbol “ $\oplus$ ” denotes the roto-translation operator  $p_V^i \oplus (\mathbf{t}, \theta) \triangleq \mathbf{R}(\theta)p_V^i + \mathbf{t}$ , where  $\mathbf{R}(\theta)$  is the 2D rotation matrix for argument angle  $\theta$ , and  $\prod \{\mathcal{S}_R, p_V^i \oplus \mathbf{q}\}$  denotes the Euclidean projector on  $\mathcal{S}_R$ .

**Remark I.** Scan-matching is employed in robotics as a means to odometry, primarily in non-wheeled robots where no encoders can be utilised, or as a useful ameliorator of the ever-drifting encoder-ed odometry: scans captured at consecutive time instances, inputted to a scan-matching algorithm, convey an estimate as to the pose of the scan sensor at the second capture time relative to that captured first. Scan-matching is being successfully employed in the tasks of simultaneous localisation and mapping [12]-[14], local map construction [15]-[17], and in people-tracking systems [18].

**Definition IV.** *Definition of a map-scan.* A map-scan is a virtual scan that encapsulates the same pieces of information as a scan derived from a physical sensor. Only their underlying operating principle is different due to the fact the map-scan refers to distances to obstacles within the map — hence its virtuality. A map-scan is captured from a virtual sensor and derived by means of locating intersections of rays emanating from the estimate of the sensor's pose and boundaries demarcating obstacles in the map.

## IV. CURRENT SOLUTIONS

## V. THE PROPOSED METHOD

The problem is iteratively decomposed into two disjunctive sub-problems. The first is estimating the relative angle between  $\mathcal{S}_1$  and  $\mathcal{S}_0$  under the assumption that both are captured from the same location. The second is estimating the relative displacement of  $\mathcal{S}_1$  with respect to  $\mathcal{S}_0$  under the

assumption that both are captured from poses of the same orientation. Solving the first sub-problem is followed by the solution to the second sub-problem. This process is iterated until termination conditions are met.

The orientation and location correction submethods are presented in subsections V-A and V-B. Subsection V-C presents the method of how these two are woven together into the system that solves Problem I that is proposed in this work.

#### A. Orientation Correction

Let the assumptions of Problem I be standing. Assume that the two scans were captured from the same location but from different orientations. Denoting with  $\mathcal{F}\{\mathcal{S}\}$  the Discrete Fourier Transform of signal  $\mathcal{S}$ , and with  $\mathcal{F}^{-1}\{\mathcal{S}\}$  its inverse, calculate  $Q_{\mathcal{S}_0, \mathcal{S}_1}$ :

$$Q_{\mathcal{S}_0, \mathcal{S}_1} \triangleq \frac{\mathcal{F}\{\mathcal{S}_0\}^* \cdot \mathcal{F}\{\mathcal{S}_1\}}{|\mathcal{F}\{\mathcal{S}_0\}| \cdot |\mathcal{F}\{\mathcal{S}_1\}|} \quad (2)$$

on the basis that if space is sampled sufficiently densely, for  $k, \xi \in [0, N_s - 1]$ ,  $k, \xi \in \mathbb{Z}$ :

$$\begin{aligned} \mathcal{S}_0[k] &\simeq \mathcal{S}_1[(k - \xi) \bmod N_s] \Leftrightarrow \\ \mathcal{F}\{\mathcal{S}_0\}(u) &\simeq e^{-j2\pi\xi u/N_s} \cdot \mathcal{F}\{\mathcal{S}_1\}(u) \end{aligned}$$

and therefore since  $2\pi \frac{\xi}{N_s} = \xi \frac{2\pi}{N_s} = \xi\gamma$

$$\begin{aligned} Q_{\mathcal{S}_0, \mathcal{S}_1}(u) &= \frac{\mathcal{F}\{\mathcal{S}_0\}^* \cdot \mathcal{F}\{\mathcal{S}_1\}}{|\mathcal{F}\{\mathcal{S}_0\}| \cdot |\mathcal{F}\{\mathcal{S}_1\}|} \\ &\simeq \frac{e^{-j\xi\gamma u} \cdot \mathcal{F}\{\mathcal{S}_1\}^* \cdot \mathcal{F}\{\mathcal{S}_1\}}{|e^{-j\xi\gamma u} \cdot \mathcal{F}\{\mathcal{S}_1\}^*| \cdot |\mathcal{F}\{\mathcal{S}_1\}|} \\ &= e^{-j\xi\gamma u} \cdot \frac{\mathcal{F}\{\mathcal{S}_1\}^* \cdot \mathcal{F}\{\mathcal{S}_1\}}{|\mathcal{F}\{\mathcal{S}_1\}| \cdot |\mathcal{F}\{\mathcal{S}_1\}|} \\ &= e^{-j\xi\gamma u} \quad (3) \end{aligned}$$

The inverse of  $Q_{\mathcal{S}_0, \mathcal{S}_1}$  is a Kronecker  $\delta$ -function  $q_{\mathcal{S}_0, \mathcal{S}_1} = \mathcal{F}^{-1}\{Q_{\mathcal{S}_0, \mathcal{S}_1}\}$  centered at  $\xi$ :

$$\xi = \arg \max_u q_{\mathcal{S}_0, \mathcal{S}_1}(u) \quad (4)$$

If the difference in orientation between the two scans is  $\Delta\theta$ , then  $\Delta\theta = \xi\gamma + \delta\theta$ , where  $\bmod(|\delta\theta|, \gamma) = \lambda \in [0, \frac{\gamma}{2}]$ . Therefore for a given number of emitted rays  $N_s$  there remains an unresolved orientation error  $|\delta\theta| \leq \gamma/2$ . The contribution of this error to the scan-matching error is two-fold, as its existence is also propagated to the location correction method. In the following, a method for further reduction of the orientation error is presented.

Let  $\mathcal{S}_0$  be projected onto the 2D plane around an arbitrary but fixed pose  $\mathbf{p}_0(x_0, y_0, \theta_0)$ , producing point-set  $\mathbf{M}_R$ , which will hereafter be referred to as the map. Then compute  $2^\nu$  map-scans (def. IV)  $\mathcal{S}_0^k$ ,  $k = 0, \dots, 2^\nu - 1$ , starting from orientation  $\theta_0$ , at  $\gamma/2^\nu$  angular increments. Then the orientation correction process is carried out once between  $\mathcal{S}_1$  and map scan  $\mathcal{S}_0^k$  taken from orientation  $\theta_0^k = \theta_0 + k \cdot \gamma/2^\nu$ , for a total of  $2^\nu$  times. An alignment metric between the  $k$ -th

map scan  $\mathcal{S}_0^k$  and scan  $\mathcal{S}_1$  is computed according to

$$\text{PD}_k = \frac{2 \max q_{\mathcal{S}_0^k, \mathcal{S}_1}}{\max q_{\mathcal{S}_0^k, \mathcal{S}_0^k} + \max q_{\mathcal{S}_1, \mathcal{S}_1}} \quad (5)$$

The Percent Discrimination metric  $\text{PD}_k \in [0, 1]$ , and is proportional to the degree of alignment between map-scan  $\mathcal{S}_0^k$  and scan  $\mathcal{S}_1$ , across all  $2^\nu$  map-scans  $\mathcal{S}_0^k$ . The above analysis is the equivalent of the 2D Fourier-Mellin Invariant matching in one dimension [23].

Let now  $K$  denote the index of the  $k$ -th map scan  $\mathcal{S}_0^K$  scoring the highest  $\text{PD}_k$ :  $\text{PD}_K = \max\{\text{PD}_k\}$ ,  $k = 0, \dots, 2^\nu - 1$ . Let also  $\Xi$  denote the integer multiple of angle increments  $\gamma$  by which  $\mathcal{S}_V^K$  should be rotated counter-clockwise in order to achieve  $\text{PD}_K$ :  $\Xi = \arg \max q_{\mathcal{S}_0^K, \mathcal{S}_1}$ . Then the sensor's orientation error is  $\Delta\theta = \Xi\gamma + K \cdot \gamma/2^\nu + \delta\theta'$ . ?? Consider CAER here ??

If map-scans  $\mathcal{S}_V^K$  were computed by raycasting the map of the environment instead of  $\mathbf{M}_R$  then the residual and unresolved orientation error  $|\delta\theta'| \in [0, \gamma/2^{1+\nu}]$ . In this case, however,  $\mathbf{M}_R$  is an approximation of the environment's map in the locality of  $\mathbf{p}_0$ . Depending on the magnitude of the sensor's angle increment and the arbitrariness of the environment, this approximation may be viewed as induced local perturbations in the map of the environment. This hold true also in the general case where  $\mathcal{S}_0$  and  $\mathcal{S}_1$  are captured from different locations. Therefore the guarantee of  $|\delta\theta'| \leq \gamma/2^{1+\nu}$  may not always hold for all combinations of environments and sensor angle increments.

#### B. Location Correction

Let the assumptions of Problem I be standing. Assume now that  $\mathcal{S}_0$  and  $\mathcal{S}_1$  were captured from different positions in the same environment but with the same orientation relative to a fixed reference frame. Let  $\mathcal{S}_0$  be projected again onto the 2D plane around fixed pose  $\mathbf{p}_0(x_0, y_0, \theta_0)$ , producing point-set  $\mathbf{M}_T$ . Assuming that  $\mathcal{S}_1$  was captured in a neighbourhood of  $\mathcal{S}_0$ , then  $\mathbf{M}_T$  is a perturbed map of the environment with respect to sensor measurement  $\mathcal{S}_1$ . Aside from measurement noise, this perturbation manifests due to the finiteness of the sensor's angle increment and to the fact that different portions of the environment are perceptible and therefore measurable from different locations [24]. Under these assumptions the problem of (scan-)matching scan  $\mathcal{S}_1$  to scan  $\mathcal{S}_0$  may be transformed into a problem of scan-to-map matching, where the aim is registering scan  $\mathcal{S}_1$  to map  $\mathbf{M}_T$ . Theorem II guarantees that the estimate of the location error between the poses from which the two scans were captured is bounded in a neighbourhood of the true location error, if the location component of the arbitrary initial pose  $\mathbf{p}_0$  is treated according to Theorem I.

**Theorem I.** *Let a 2D range scan  $\mathcal{S}_R$  be captured from a physical panoramic range sensor from unknown pose  $\mathbf{p} = (\mathbf{l}, \theta)$ ,  $\mathbf{l} = (x, y)$ . Let  $\mathbf{M}$  be the map of the world in which the scan was captured. Let a pose estimate  $\hat{\mathbf{p}} = (\hat{\mathbf{l}}, \hat{\theta})$  reside in the neighbourhood of  $\mathbf{p}$  in the map's frame of reference. Additionally, let  $\hat{\theta} = \theta$ . Assume that  $\mathcal{S}_R$  is disturbance-*

free, and that the map of the environment captures the latter perfectly. Then, treating the estimate of the location of the sensor as a state variable  $\hat{\mathbf{l}}[k] = [\hat{x}[k], \hat{y}[k]]^\top$  and updating it according to the difference equation

$$\hat{\mathbf{l}}[k+1] = \hat{\mathbf{l}}[k] + \mathbf{u}[k] \quad (6)$$

where  $\hat{\mathbf{l}}[0] = \hat{\mathbf{l}} = [\hat{x}, \hat{y}]^\top$ , i.e. the supplied initial location estimate, where

$$\mathbf{u}[k] = \frac{1}{N_s} \begin{bmatrix} \cos \hat{\theta} & \sin \hat{\theta} \\ \sin \hat{\theta} & -\cos \hat{\theta} \end{bmatrix} \begin{bmatrix} X_{1,r}(S_R, S_V | \hat{\mathbf{p}}[k]) \\ X_{1,i}(S_R, S_V | \hat{\mathbf{p}}[k]) \end{bmatrix} \quad (7)$$

is the two-dimensional vector hereafter referred to as the control vector, with  $X_{1,r}(\cdot)$  and  $X_{1,i}(\cdot)$  being, respectively, the real and imaginary parts of the complex quantity  $X_1$ :

$$\begin{aligned} X_1(S_R, S_V | \hat{\mathbf{p}}[k]) &= X_{1,r}(S_R, S_V | \hat{\mathbf{p}}[k]) \\ &\quad + i \cdot X_{1,i}(S_R, S_V | \hat{\mathbf{p}}[k]) \\ &= \sum_{n=0}^{N_s-1} (S_R[n] - S_V[n] | \hat{\mathbf{p}}[k]) \cdot e^{-i \frac{2\pi n}{N_s}} \quad (8) \end{aligned}$$

where  $S_R[n]$  and  $S_V[n] | \hat{\mathbf{p}}[k]$  are, respectively, the ranges of the  $n$ -th ray of real scan  $S_R$  and map-scan  $S_V | \hat{\mathbf{p}}[k]$  captured via raycasting the map  $M$  from  $\hat{\mathbf{p}}[k] = (\hat{\mathbf{l}}[k], \hat{\theta})$ —then  $\hat{\mathbf{l}}[k]$  converges to  $\mathbf{l}$  uniformly asymptotically as  $k \rightarrow \infty$ .

**Theorem II.** Let the assumptions of Theorem I hold. Assume additionally that the ranges of both real and virtual range scans  $S_R$  and  $S_V$  are affected by additive, bounded disturbances. Then  $\hat{\mathbf{l}}[k]$  is uniformly bounded for  $k \geq k_0$  and uniformly ultimately bounded in a neighbourhood of  $\mathbf{l}$ . Its size depends on the suprema of the disturbance corrupting the range measurements of the two scans.

### C. Pose correction

The previous two sections describe two methods of how it is possible to (a) reduce the error of the orientation estimate when the position estimate coincides with the sensor's position, and (b) reduce the error of the position estimate when the orientation estimate equals the sensor's orientation. In the general case, however, no equality stands. What is more is that the problem is coupled: the optimal orientation error cannot be attained in one step when the position error is not zero, and the optimal position error cannot be attained in one step when the orientation error is not zero. Therefore the first goal of a method reducing both would be to first reduce the orientation error and then reduce the location error. The second would be to iterate this process until some termination condition is met. This method is described in the following.

Given an input pose estimate  $\hat{\mathbf{p}}(\hat{x}, \hat{y}, \hat{\theta})$ , the real scan  $S_R$ , and the map  $M$ , the pose correction method proposed (fig. ??) reduces the error of the pose estimate by iteratively invoking the One-step Pose Correction process (fig. ??) until a set of termination conditions is met. Denoting the former by FSMSM, FSMSM starts off with an initial degree of sampling the map  $\nu = \nu_{\min}$ . The input pose estimate is processed by the One-step Pose Correction process, and its output  $\hat{\mathbf{p}}'$  is examined with regard to Recovery and

Convergence conditions. If the resulting pose estimate falls outside of the map  $M$  then a new pose estimate is generated from the initially supplied pose estimate, and the process is reset. If no significant pose estimate correction is observed  $\|\hat{\mathbf{p}}' - \hat{\mathbf{p}}\|_2 < \varepsilon_{\delta p}$ , then the degree of map sampling  $\nu$  is increased. Its increase serves as a means of reducing the orientation and hence the position estimate error further. Otherwise, the One-step Pose Correction process is reiterated until no significant correction is observed. The process is iterated until a maximum degree of map sampling is reached  $\nu = \nu_{\max}$ , at which point FSMSM terminates if a terminal condition is met. This terminal condition facilitates the avoidance of local maxima. In the case where this condition is not met, a new pose is generated, and the process is reset.

Given an input pose estimate  $\hat{\mathbf{p}}(\hat{x}, \hat{y}, \hat{\theta})$ , the real scan  $S_R$ , the map  $M$ , and a sampling degree  $\nu$ , the One-step Pose Correction system first calculates  $2^\nu$  pose estimates  $\hat{P}_{OC} = \{(\hat{x}_k, \hat{y}_k, \hat{\theta}_k)\}$ ,  $k = 0, \dots, 2^\nu - 1$ . The Orientation Correction system utilises Algorithm ?. Its operation is denoted in fig. ?? by the operator OC( $\cdot$ ).

Now, if the position of the input pose estimate coincided with the position of the real sensor, the Percent Discrimination metric (eq. 5) would suffice in serving as an accurate determinant of the pose estimate with the least orientation error. In practice, however, the ranking provided by the Percent Discrimination metric is confounded by the incoincidence of the two positions. In order to mitigate this effect, each pose estimate in  $\hat{P}_{OC}$  is given over to the Position Correction system, where the position of each pose estimate is displaced once ( $I=1$ ), according to Algorithm ?. This operation, denoted by the operator RPC( $\cdot$ ) in fig. ??, produces the set  $\hat{P}_{RPC} = \{(\hat{x}_k, \hat{y}_k, \hat{\theta}_k)\}$ ,  $|\hat{P}_{RPC}| = 2^\nu$ . The purpose of this operation is for it to provide an advance view of the next step of position correction: the less rotationally misaligned a pose estimate is, the less it will diverge in terms of orientation and hence position with respect to the sensor's actual pose once inputted to the position correction system. This divergence is captured by the Cumulative Absolute Error per Ray (CAER) metric:

$$\text{CAER}_k = \sum_{n=0}^{N_s-1} \left| S_R[n] - S_V[n] \right|_{(\hat{x}_k, \hat{y}_k, \hat{\theta}_k)} \quad (9)$$

where  $k = 0, \dots, 2^\nu - 1$ . The CAER metric encodes at the same time a degree of alignment of position and orientation between its two input scans.<sup>1</sup> By rehearsing the position correction of each pose estimate in  $\hat{P}_{OC}$  and capturing the CAER for each of its displaced pose estimates in  $\hat{P}_{RPC}$ , it is possible to establish a pose error rank between pose estimates in  $\hat{P}_{OC}$  and simultaneously retain only one pose estimate for the next iteration of the One-step Pose Correction method.<sup>2</sup> The pose estimate  $\hat{\mathbf{p}}_C \in \hat{P}_{OC}$  that, when translated once,

<sup>1</sup>By contrast, dropping the absolute value operator would provide only for a position alignment metric.

<sup>2</sup>Alternatively, correcting the position of  $2^\nu$  pose estimates and feeding them back to the One-step Pose Correction method would incur exponential costs in time of execution.

records the minimum CAER among all similarly-treated pose estimates in  $\hat{P}_{OC}$  is inputted to the Position Correction method proper. The number of translation iterations  $I$  it undergoes is an increasing function in the degree of map sampling  $\nu$ .<sup>3</sup> The Position Correction system produces  $\hat{p}'$ , which is then fed back to the Orientation Correction system in the form of its new pose estimate  $\hat{p} \leftarrow \hat{p}'$ . In practice, the pose set  $\hat{P}_{OC}$  is supplemented with one pose whose position is equal to  $\hat{p}$  and whose orientation is equal to the orientation of  $\hat{p}_C$  that produces the minimum CAER over time. This addition introduces a form of memory to the system, which assists it in avoiding divergence and which, therefore, benefits speed of execution.

## VI. EXPERIMENTAL PROCEDURE

This section serves to test the efficacy and performance of the proposed method. The experimental procedure was conducted using a benchmark dataset  $D$  consisting of  $|D| = 778$  laser scans obtained from a Sick range-scan sensor mounted on a robotic wheel-chair.<sup>4</sup> For each scan  $D^d$ ,  $d = 1, \dots, 778$ , the dataset reports one range scan of 360 range measurements and the pose from which it was captured  $r^d(x, y, \theta)$ . The same dataset was used to evaluate the performance of IDC [21], ICP, and MBICP in [3], and that of PLICP and the joint method PLICP◦GPM during scan-matching experiments. In [4] the latter was found to be the best-performing among the five correspondence-finding scan-matching methods. Therefore for purposes of comparison against correspondence-finding scan-matching methods that may be utilised in scan-to-map-scan matching, the experimental procedure is extended to PLICP◦GPM. This method shall be denoted hereafter by the acronym CSM. In the same vein, for purposes of comparison against correspondenceless scan-matching methods, the same experimental procedure is extended to the Normal Distributions Transform (NDT) scan-matching method [10].

The experimental setup is the following. The rays of each dataset instance  $D^d$  are first projected to the  $x - y$  plane around  $r^d$ . The dataset's scans are not panoramic, therefore the remaining space is filled with a semicircular arc that joins the scan's two extreme ends. Its radius is set to the minimum range between the two extreme rays of  $D^d$ . Similar fashions for closing-off the environment have been found equivalent with respect to the performance of the tested methods. The resulting point-set is regarded as the environment  $W^d$  in

<sup>3</sup>The rationale of chaining the number of translational iterations to the map sampling degree  $\nu$  is the following. Since the orientation error is inversely proportional to  $\nu$ , at low map sampling rates, when the position estimate error is at its highest, if the number of translational iterations was high then the position estimate would be susceptible to divergence. Therefore the number of translational iterations is kept low at initial stages so that a balance between decreasing position error and position divergence is struck. At higher values of  $\nu$ , the orientation estimate error decreases, and then divergence is bounded and/or met at higher translational iteration values. As the orientation estimate becomes ever more accurate, the Position Correction system is let to iterate more times so that further reduction of the position error be feasible.

<sup>4</sup>The dataset is available at <https://censi.science/pub/research/2007-plicip/laserazosSM3.log.gz>

which the range sensor operates (e.g. the environment of fig. ??). Then the map of the environment  $M^d$  is set to be  $W^d$ . In order to induce distortions in the map, each coordinate of all points in  $M^d$  is perturbed by errors extracted from a normal distribution  $\mathcal{N}_M \sim (0, \sigma_M^2)$ . What is considered the sensor's actual pose  $p^d$  is generated randomly within the polygon formed by  $W^d$ . The range scan  $\mathcal{S}_R^d$  that is considered to be reported by the physical sensor is then computed by locating the intersection points between  $N_s$  rays emanating from  $p^d$  and the polygon formed by  $W^d$  across an angular field of view  $\lambda = 2\pi$ . The initial pose estimate of the sensor  $\hat{p}^d$  is then obtained by perturbing the components of  $p^d$  with quantities extracted from uniformly distributed error distributions  $U_{xy}(-\bar{\delta}_{xy}, \bar{\delta}_{xy})$ ,  $U_\theta(-\bar{\delta}_\theta, \bar{\delta}_\theta)$ ;  $\bar{\delta}_{xy}, \bar{\delta}_\theta \in \mathbb{R}_{\geq 0}$ .

In order to test for the performance of the proposed method, four levels of noise acting on the range measurements of the real scan  $\mathcal{S}_R^d$  are tested. The range measurements are perturbed by zero-mean normally-distributed noise with standard deviation  $\sigma_R \in \{0.01, 0.03, 0.05, 0.10\}$  m.<sup>5</sup> In addition, two levels of map distortion are tested:  $\sigma_M \in \{0.0, 0.05\}$  m.

For each experiment FSMSM, CSM, and NDT ran for  $E = 100$  times across all instances of  $D$ . CSM was set up as follows. GPM [22] was used initially in order to overcome the angular realignment problems [4] of PLICP. Then PLICP was executed for  $I_{PLICP}$  times, and the total matching error (eq. 1) was recorded. The pose estimate returned was that which scored the lowest matching error across  $I_{PLICP}$  iterations. GPM was called once because it was found to be impedimental to convergence at medium to high levels of noise when called iteratively. NDT was run for  $I_{NDT}$  iterations. FSMSM's termination criterion was set to  $CAER(\hat{p}') \leq (\hat{\sigma}_R + \hat{\sigma}_V)^{1/2}$ , where  $\hat{\sigma}_R$  and  $\hat{\sigma}_V$  are estimates of the standard deviation of noise affecting the rays of  $\mathcal{S}_R$  and  $\mathcal{S}_V$  respectively. All experiments and algorithms were run serially, on a single thread, on a machine with a CPU frequency of 4.0 GHz.

The criterion on which the evaluation of all tests rests is the 2-norm of the total pose error—eq. (??) for  $\hat{p} \rightarrow \hat{p}'$ , where  $\hat{p}'$  is the output of each algorithm tested. For every pose estimate  $\hat{p}'_d$  outputted by each algorithm,  $d = 1, 2, \dots, |D|$ , its offset from the actual pose  $p^d$  is recorded in the form of the 2-norm total error. The pose errors of one simulation are then averaged. The pose error distributions reported below are those of mean errors across  $E$  simulations of the same configuration. The unit of measurement of the total pose error is  $(m^2 + rad^2)^{1/2}$ , and it is omitted in the figures of the following subsections for reasons of economy

<sup>5</sup>The values of tested standard deviations were calculated from commercially available panoramic LIDAR scanners by identifying the magnitude of their reported maximum range errors and dividing it by a factor of three. The rationale is that 99.73% of errors are located within  $3\sigma$  around the actual range between a ray and an obstacle, assuming errors are distributed normally. The minimum standard deviation  $\sigma_R = 0.01$  m is reported for VELODYNE sensors [25]; the rest are reported for price-appealing but disturbance-laden sensors, e.g. the RPLIDAR A2M8, or the YDLIDAR G4, TG30, and X4 scanners [26]–[29]

# Distribution of mean pose errors — $\sigma_M = 0.0$ m

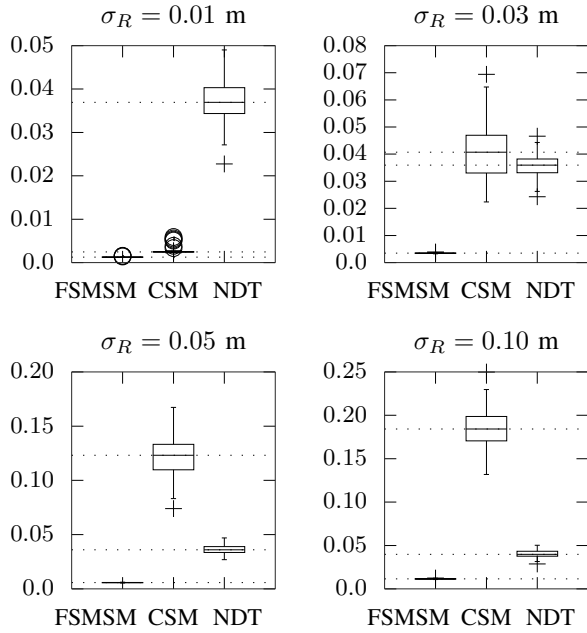


Fig. 1: Pose errors of FSMSM, CSM, and NDT for maximal uniform position displacements  $\delta_{xy} \in U_{xy}(-0.20, +0.20)$  m and maximal uniform orientation displacements  $\delta_\theta \in U_\theta(-\pi/4, +\pi/4)$  rad for  $\sigma_M = 0.0$  m over  $E = 100$  runs per noise level tested  $\sigma_R$

of space.

Figures 1 and ?? show the distribution of the three methods' mean pose errors across  $E$  experiments for maximal displacements  $\bar{\delta}_{xy} = 0.20$  m and  $\bar{\delta}_\theta = \pi/4$  rad, when  $\sigma_M = 0.0$  m and  $\sigma_M = 0.05$  m respectively. The value of  $\bar{\delta}_{xy}$  was chosen as such from reports on positional errors in real conditions [?]. The value of  $\bar{\delta}_\theta$  was chosen as such in order to include orientation errors at the initialisation stage of pose tracking. The size of the input real scan was set to  $N_s = 360$  rays. The minimum and maximum oversampling rates of FSMSM were set to  $(\mu_{\min}, \mu_{\max}) = (2^{\nu_{\min}}, 2^{\nu_{\max}}) = (2^2, 2^5)$ . The number of iterations of the translational component at each map sampling degree  $\nu$  was set at  $I = 2\nu$ . The number of iterations of PLICP and NDT were set to  $I_{\text{PLICP}} = I_{\text{NDT}} = 10$ ; higher values did not yield improved results.

## VII. DISCUSSION

## VIII. CONCLUSIONS

## REFERENCES

- [1] Sebastian Thrun, Wolfram Burgard, and Dieter Fox, "Probabilistic Robotics" (Intelligent Robotics and Autonomous Agents), The MIT Press, 2005
- [2] P. J. Besl and N. D. McKay, "A method for registration of 3-D shapes", IEEE Transactions on Pattern Analysis and Machine Intelligence, 1992, volume 14, number 2, pp. 239-256, doi 10.1109/34.121791, ISSN 0162-8828
- [3] J. Minguez, F. Lamiroux and L. Montesano, "Metric-Based Scan Matching Algorithms for Mobile Robot Displacement Estimation," Proceedings of the 2005 IEEE International Conference on Robotics and Automation, Barcelona, Spain, 2005, pp. 3557-3563, doi: 10.1109/ROBOT.2005.1570661

- [4] A. Censi, "An ICP variant using a point-to-line metric," 2008 IEEE International Conference on Robotics and Automation, Pasadena, CA, 2008, pp. 19-25, doi: 10.1109/ROBOT.2008.4543181. Code available at <https://github.com/AndreaCensi/csm>
- [5] Wang, J. Zhao, M. Chen, W. "MIM-SLAM: A Multi-Level ICP Matching Method for Mobile Robot in Large-Scale and Sparse Scenes". Appl. Sci. 2018, 8, 2432.
- [6] Tian, Yingzhong; Liu, Xining; Li, Long; Wang, Wenbin. 2019. "Intensity-Assisted ICP for Fast Registration of 2D-LIDAR" Sensors 19, no. 9: 2124.
- [7] Naus, Krzysztof; Marchel, ukasz. 2019. "Use of a Weighted ICP Algorithm to Precisely Determine USV Movement Parameters" Appl. Sci. 9, no. 17: 3530.
- [8] Linh Tao, Tam Bui, Toshio Ito, "MODIFIED ITERATIVE CLOSEST POINT MATCHING FOR 2D LIDAR LASER DATA", 14th South East Asian Technical University Consortium 2020 (SEATUC 2020) 27th 28th February 2020, KX Building, KMUTT, Bangkok, Thailand
- [9] Huchao Xu, Letao Zhou, Yinghao Zhao, Zheng Yuan, "A Two-Dimensional Point Cloud Matching Method Based on ICP Improvement", China Satellite Navigation Conference (CSNC) 2020 Proceedings: Volume I pp 390-398
- [10] P. Biber and W. Strasser, "The normal distributions transform: a new approach to laser scan matching," Proceedings 2003 IEEE/RSJ International Conference on Intelligent Robots and Systems (IROS 2003) (Cat. No.03CH37453), Las Vegas, NV, USA, 2003, pp. 2743-2748 vol.3, doi: 10.1109/IROS.2003.1249285.
- [11] Cooper, M.A.; Raquet, J.F.; Patton, R. Range Information Characterization of the Hokuyo UST-20LX LIDAR Sensor. Photonics 2018, 5, 12.
- [12] J. -. Gutmann and K. Konolige, "Incremental mapping of large cyclic environments" Proceedings 1999 IEEE International Symposium on Computational Intelligence in Robotics and Automation. CIRA'99 (Cat. No.99EX375), Monterey, CA, USA, 1999, pp. 318-325. doi: 10.1109/CIRA.1999.810068
- [13] D. Hahnel, W. Burgard, D. Fox and S. Thrun, "An efficient fastSLAM algorithm for generating maps of large-scale cyclic environments from raw laser range measurements," Proceedings 2003 IEEE/RSJ International Conference on Intelligent Robots and Systems (IROS 2003) (Cat. No.03CH37453), Las Vegas, NV, USA, 2003, pp. 206-211 vol.1. doi: 10.1109/IROS.2003.1250629
- [14] Chieh-Chih Wang, C. Thorpe and S. Thrun, "Online simultaneous localization and mapping with detection and tracking of moving objects: theory and results from a ground vehicle in crowded urban areas," 2003 IEEE International Conference on Robotics and Automation (Cat. No.03CH37422), Taipei, Taiwan, 2003, pp. 842-849 vol.1. doi: 10.1109/ROBOT.2003.1241698
- [15] Lacroix, S., Mallet, A., Bonnafous, D., Bauzil, G., Fleury, S., Herrb, M., and Chatila, R. (2002). "Autonomous Rover Navigation on Unknown Terrains: Functions and Integration". The International Journal of Robotics Research, 21(1011), 917942. <https://doi.org/10.1177/027836490201010841>
- [16] Minguez, J., Montesano, L., and Montano, L. (2004). "An architecture for sensor-based navigation in realistic dynamic and troublesome scenarios". 2004 IEEE/RSJ International Conference on Intelligent Robots and Systems (IROS) (IEEE Cat. No.04CH37566), 3, 2750-2756 vol.3.
- [17] Montesano, Luis, Minguez, Javier and Montano, Luis, "Modeling dynamic scenarios for local sensor-based motion planning", Autonomous Robots, 2008, Volume 25, pp 231-251.
- [18] D. Schulz, W. Burgard, D. Fox and A. B. Cremers, "Tracking multiple moving targets with a mobile robot using particle filters and statistical data association", Proceedings 2001 ICRA. IEEE International Conference on Robotics and Automation (Cat. No.01CH37164), Seoul, South Korea, 2001, pp. 1665-1670 vol.2. doi: 10.1109/ROBOT.2001.932850
- [19] M. Leordeanu and M. Hebert, "A spectral technique for correspondence problems using pairwise constraints", Tenth IEEE International Conference on Computer Vision (ICCV'05) Volume 1, Beijing, 2005, pp. 1482-1489 Vol. 2. doi: 10.1109/ICCV.2005.20
- [20] Filotheou, A., Tsardoulas, E., Dimitriou, A. et al. "Pose Selection and Feedback Methods in Tandem Combinations of Particle Filters with Scan-Matching for 2D Mobile Robot Localisation". J Intell Robot Syst 100, 925944 (2020). <https://doi.org/10.1007/s10846-020-01253-6>
- [21] Feng Lu and Milios, "Robot pose estimation in unknown environments by matching 2D range scans," 1994 Proceedings of IEEE Conference

- on Computer Vision and Pattern Recognition, Seattle, WA, USA, 1994, pp. 935-938.
- [22] A. Censi, "Scan matching in a probabilistic framework," Proceedings 2006 IEEE International Conference on Robotics and Automation, 2006. ICRA 2006., Orlando, FL, 2006, pp. 2291-2296, doi: 10.1109/ROBOT.2006.1642044.
  - [23] Qin-Sheng Chen, M. Defrise and F. Deconinck, "Symmetric phase-only matched filtering of Fourier-Mellin transforms for image registration and recognition," in IEEE Transactions on Pattern Analysis and Machine Intelligence, vol. 16, no. 12, pp. 1156-1168, Dec. 1994, doi: 10.1109/34.387491.
  - [24] E. B. Olson, "Real-time correlative scan matching," 2009 IEEE International Conference on Robotics and Automation, Kobe, Japan, 2009, pp. 4387-4393, doi: 10.1109/ROBOT.2009.5152375.
  - [25] VELODYNE sensors' datasheet <https://visimind.com/wp-content/uploads/2018/12/LiDAR-Product-Brochure.pdf>
  - [26] RPLIDAR A2M8 datasheet [https://cdn.sparkfun.com/assets/e/a/f/9/8/LD208\\_SLAMTEC\\_rplidar\\_datasheet\\_A2M8\\_v1.0\\_en.pdf](https://cdn.sparkfun.com/assets/e/a/f/9/8/LD208_SLAMTEC_rplidar_datasheet_A2M8_v1.0_en.pdf)
  - [27] YDLIDAR G4 datasheet <https://www.ydlidar.com/Public/upload/files/2020-10-29/YDLIDAR%20G4%20Datasheet.pdf>
  - [28] YDLIDAR TG30 datasheet <https://www.ydlidar.com/Public/upload/files/2020-10-13/YDLIDAR%20TG30%20Data%20sheet.pdf>
  - [29] YDLIDAR X4 datasheet <https://www.ydlidar.com/Public/upload/files/2020-04-13/YDLIDAR%20X4%20Datasheet.pdf>
  - [30] F.A. Donoso, K.J. Austin, P.R. McAree, "How do ICP variants perform when used for scan matching terrain point clouds?," Robotics and Autonomous Systems, Volume 87, 2017, Pages 147-161, ISSN 0921-8890, <https://doi.org/10.1016/j.robot.2016.10.011>.